Contents list available at IJRED website

Int. Journal of Renewable Energy Development (IJRED)

Journal homepage: https://ijred.undip.ac.id

Research Article

Improved Evaluation of The Wind Power Potential of a Large Offshore Wind Farm Using Four Analytical Wake Models

Mohammed Amine Hassoine[a*], Fouad Lahlou[a], Adnane Addaim[b], Abdessalam Ait Madi[c]

[a] Faculty of Sciences, Ibn Tofail University, Kenitra, Morocco

[b] Mohammadia School of Engineers, Mohammed Vth University in Rabat, Morocco

[c] National School of Applied Sciences, Ibn Tofail University, Kenitra, Morocco

Abstract. The objective of this paper is to investigate the ability of analytical wake models to estimate the wake effects between wind turbines (WTs). The interaction of multiple wakes reduces the total power output produced by a large offshore wind farm (LOFWF). This power loss is due to the effect of turbine spacing (WTS), if the WTs are too close, the power loss is very significant. Therefore, the optimization of turbine positions within the offshore wind farm requires an understanding of the interaction of wakes inside the wind farm. To better understand the wake effect, the Horns Rev 1 offshore wind farm has been studied with four wake models, Jensen, Larsen, Ishihara, and Frandsen. A comparative study of the wake models has been performed in several situations and configurations, single and multiple wakes are taken into consideration. Results from the Horns Rev1 offshore wind farm case have been evaluated and compared to observational data, and also with the previous studies. The power output of a row of WTs is sensitive to the wind direction. For example, if a row of ten turbines is aligned with the 270° wind direction, the full wake condition of WTs is reached and the power deficit limit predicted by Jensen model exceeds 70%. When a wind direction changes only of 10° (260° and 280°), the deficit limit reduces to 30%. The obtained results show that a significant power deficit occurs when the turbines are arranged in an aligned manner. The findings also showed that all four models gave acceptable predictions of the total power output. The comparison between the calculated and reported power output of Horns Revs 1 showed that the differences ranged from - 8.27 MW (12.49%) to 15.27 MW (23.06%) for the Larsen and Frandsen models, respectively.

Keywords: Offshore wind farm, Wind turbine, Wake model, velocity deficit, wind speed, wind direction.

Article History: Received: 5th May 2021; Revised: 19th July 2021; Accepted: 30th August 2021; Available online: 10th September 2021
How to Cite This Article: Hassoine, M.A., Lahlou, F., Addaim, A., Madi, A.A. (2022) Improved Evaluation of The Wind Power Potential of a Large Offshore Wind Farm Using Four Analytical Wake Models. *International Journal of Renewable Energy Development*, 11(1), 35-48. https://doi.org/10.14710/ijred.2022.38263

1. Introduction

WTs are organized into a wind farm (WF), which includes a set that goes from a few units up to almost two hundred WTs. The WF is scattered overland (Onshore Wind Farm) or sea (Offshore Wind Farm) at sites carefully selected based on wind potential. To maximize the electrical energy produced by a WF, wind turbines should be spaced in the direction of the prevailing winds, so that they can continue to receive strong winds.

The wake downstream of the WTs is characterized by high-speed deficit and turbulence which affect the performance of the wind turbines. The wake is divided into two main regions (Vermeer *et al*. 2003): the near wake and the far wake. In the first region, the generation of turbulence is associated with eddies created by WTs. It ends at a downstream distance between 2D and 4D (D is the diameter of the rotor) (Machefaux 2015). In the distant wake, ambient turbulence is the factor that primarily affects the rate of wake growth. Between them, there is an intermediate zone that can be estimated from 5D to 7D (Brun *et al.* 2004, García *et al.* 2017) showed that the wake keeps a similar speed profile behind the turbine between 6D and 15D.

For an assessment of the losses of the power wind farm, it is necessary to model the wake effects of WTs at the scale of the WF. One way to predict the deficit in the wake of a turbine is to use computational fluid dynamics (CFD). The main approach of CFD is to use the Actuator Disc (AD) model (Crasto *et al.* 2012, Richmond *et al.* 2019), in which the surface of a turbine is represented by a porous disc. The CFD models give high accuracy, but require a lot of resources and involve considerable computation time to calculate the flux field for a WF, and therefore to find the optimal layout of the wind farm.

Another way is the use of analytical models to calculate the expansion and wake velocity deficits in more complex situations without having recourse to CFD. In this context, these models allow the prediction of the mean speed deficit in the wake of WTs. Some typical analytical models of wake modeling have been conducted by (Jensen

* Corresponding author: mohamedamine.hassoine@uit.ac.ma

1983, Larsen 1988, Ishihara et al. 2004, Frandsen *et al.* 2006, Bastankhah & Porté-Agel 2014). However, analytical models are less accurate than CFD simulation methods, but they can provide an acceptable representation that is very suitable for describing the behavior of the wake. Other alternatives based on Jensen's model, use a Cosine (Tian et al. 2015) or Gaussian shape function (Gao *et al.* 2016) to describe the deficit taking into account the speed variation in the radial direction of the turbine.

Many studies have been carried out by different researchers to evaluate the wind energy output of the WF by using different wake models. Tong et al. (Tong et al. 2012) investigated the impact of four analytical wake models on the estimated power output of a WF. Göçmen *et al.* (Göçmen *et al.* 2016) evaluated six wake models using data from the Sexbierum onshore and Lill-grund offshore wind farms. Sun & Yanga (Sun & Yanga 2018) estimated offshore wind energy output in Hong Kong by using three wake models. Hamilton *et al.* (Hamilton *et al.* 2020) examined seven wake models and compared the results with observational data from the Lillgrund Wind Plant.

In this paper, the Horns Rev 1 OWF in Denmark is invested with Jensen, Larsen, Ishihara, and Frandsen wake models. The aim is to assess both, the ability of the four models to predict the behavior of aligned and misaligned wakes for a row of ten turbines, and the efficiency of all turbines of the offshore wind farm (OWF). These four models have been also evaluated through the calculation of the output power of Horns Rev 1. To simulate the different cases studied, MATLAB software has been used to perform the simulations.

The remaining of this paper is organized as follows. The mathematical description of the wake models, the calculation of the power of the wind farm are discussed in section 2. The presentation of the Horns Rev1 OWF and the wind characteristics are presented in section 3. In section 4, the simulations of wake speed, power deficit, and efficiency are studied and discussed. Section 5 presents the conclusions.

2. Mathematical Wake Models and Power Calculation

In this paragraph, a description of the four analytical wake models and mathematical formulations is presented. Especially, the Jensen, Larsen, Ishihara, and Frandsen models are treated in the present study.

2.1. Jensen Wake Model

This wake model was developed by the Risø laboratory in Denmark (Jensen 1983, Katic *et al.* 1987). In this model, the wake behind the turbine has a starting diameter assumed to be equal to the downstream diameter of the turbine and propagates linearly as a function of the distance crossing by the wind. The expression for the velocity deficit is given by Equation (1):

$$\frac{u_w(x)}{u_0} = 1 - \frac{2a}{\left(1 + 2\alpha\left(x / D_r\right)\right)^2} \tag{1}$$

Where u_0 is the mean wind speed, x is the downstream distance, a is the axial induction factor, and D_r is the downstream rotor diameter of the turbine.

The decay factor α describes how the wake expands. The wake width is defined by Equation (2):

$$D_w(x) = D_r + 2\alpha x \tag{2}$$

The wake expansion coefficient (decay factor) depends on the hub height (Z) and the surface roughness height (Z_0). This decay factor can be calculated by using Equation (3) (Frandsen 1992):

$$\alpha = \frac{0.5}{\ln\left(z / z_0\right)} \tag{3}$$

The downstream rotor diameter (D_r) of the turbine is related to the wind turbine rotor diameter (D) through the Betz relations (Frandsen 1992):

$$D_r = D\sqrt{\frac{(1-a)}{(1-2a)}} \quad ; a = \frac{1-\sqrt{1-C_T}}{2} \tag{4}$$

Here, C_T is the thrust coefficient of the turbine. When the wakes of the turbines are not completely aligned, the speed deficit can be calculated as a ratio of the wake interference area ($S_{overlap}$) of an upstream turbine to a downstream turbine rotor area (S_0) as shown in Equation (5):

$$\frac{u_w(x)}{u_0} = 1 - \frac{2a}{\left(1 + 2\alpha\left(x / D_r\right)\right)^2}\left(\frac{S_{overlap}}{S_0}\right) \tag{5}$$

where $S_{overlap}$ is the wake swept area and S_0 is the rotor swept area.

2.2. Frandsen Wake Model

The Frandsen wake model is designed to predict the wind speed deficit in large rectangular offshore wind farms with constant row spacing. It was presented at the European Wind Energy 2006 conference and exhibition (Frandsen et al. 2006). The model shows three different wake regimes. In the first regime, single or multiple wakes are present without interaction between adjacent wakes. The second regime begins when the neighboring wakes interact. The third regime is in equilibrium with the planetary boundary layer, the third regime is in equilibrium with the planetary boundary layer. This happens in very large offshore wind farms. In a single wake, the velocity deficit is given by Equation (6):

$$\frac{u_w(x)}{u_0} = 1 - \left[\frac{1}{2}\left(1 - \sqrt{1 - 2\frac{A_0}{A_w}C_T}\right)\right] \tag{6}$$

where A_0 is the swept area of the rotor and A_w is the area of the wake.

The wake width can be expressed by Equation (7):

$$D_w(x) = D\left(\beta^{\frac{k}{2}} + \left(\alpha x / D\right)\right)^{\frac{1}{k}} \tag{7}$$

Here, the value of k equals 2 if the square root shape is chosen (Frandsen *et al.* 2006), and ß is the expansion parameter given by Equation (8):

$$\beta = \left(1+\sqrt{1-C_T}\right)/\left(2\sqrt{1-C_T}\right) \tag{8}$$

2.3. Larsen Wake Model

The G.C. Larsen wake model is semi-analytical (Larsen 1988, Larsen 2009) and is also developed by the Risø laboratory. It first assumes that the wake behind a wind turbine (WT) can be adequately described by the turbulent boundary layer Equations of Prandtl. These Equations can be considered as an asymptotic version of the Equations of Navier-Stokes for a high Reynold number. The G.C. Larsen model neglects wind shear to be able to express the boundary layer Equations in the form of cylindrical coordinates. Finally, the fluid is assumed to be incompressible.

The mean wind speed deficit in the wake, and the wake diameter, are expressed by Equations (9) and (10):

$$\frac{u_w(x,r)}{u_0} = 1 - \frac{1}{9}\left(C_T A_0 \left(x+x_0\right)^{-2}\right)^{\frac{1}{3}} \times \left(r^{\frac{3}{2}}\left(3c_1^2 C_T A_0 \left(x+x_0\right)\right)^{-\frac{1}{2}} - \left(\frac{35}{2\pi}\right)^{\frac{3}{10}}\left(3c_1^2\right)^{-\frac{1}{5}}\right)^2 \tag{9}$$

$$D_w(x) = 2\left(\frac{105}{2\pi}c_1^2\right)^{\frac{1}{5}}\left(C_T A_0 \left(x+x_0\right)\right)^{\frac{1}{3}} \tag{10}$$

where x and r indicated axial and radial directions, A_0 is the rotor area, C_T is the rotor thrust coefficient, u_0 mean wind velocity at hub height, and c_1 is the non–dimensional mixing length expressed by using Equations (11) and (12):

$$c_1 = \left(\frac{D_{eff}}{2}\right)^{\frac{5}{2}}\left(\frac{105}{2\pi}\right)^{-\frac{1}{2}}\left(C_T A_0 x_0\right)^{-\frac{5}{6}} \tag{11}$$

where x_0 is a constant which determines the position of the rotor inadequacy with the coordinate system for $x_0 > 0$.

$$x_0 = \frac{9.5D}{\left(\frac{2R_{9.5}}{D_{eff}}\right)^3 - 1} \tag{12}$$

where D_{eff} is the effective rotor diameter expressed by Equation (13):

$$D_{eff} = D\sqrt{\frac{1+\sqrt{1-C_T}}{2\sqrt{1-C_T}}} \tag{13}$$

And R9.5 represents the wake radius at a distance of 9.5 times the rotor diameter (9.5D) behind the turbine and is determined by Equations (14) and (15):

$$R_{9.5} = 0.5\left(R_{nb} + \min\left(H, R_{nb}\right)\right) \tag{14}$$

With

$$R_{nb} = \max\left(1.08D, 1.08D + 21.7D\left(I_a - 0.05\right)\right) \tag{15}$$

H is the hub height and I_a is the ambient turbulence intensity.

2.4 Ishihara Wake Model

The Ishihara model (Ishihara et al. 2004) was developed using wind tunnel data for a 1/100 scale of a Mitsubishi WT. The model takes into account the effect of turbulence on wake recovery, allowing the model to be adapted to different conditions. The velocity profile is assumed to be described as a Gaussian shape. The speed deficit is given by Equation (16):

$$\frac{u_w(x,r)}{u_0} = \frac{C_T^{\frac{1}{2}}}{32}\left(\frac{1.666}{k_1}\right)^2\left(\frac{x}{D}\right)^{-P}\exp\left(-\frac{r^2}{b^2}\right) \tag{16}$$

where x and r indicate, respectively axial and radial directions, D is the rotor diameter of the turbine and C_T is the thrust coefficient. The wake growth is described by Equation (17):

$$b(x) = \frac{k_1 C_T^{\frac{1}{4}}}{0.833} d^{1-\frac{p}{2}} x^{\frac{p}{2}} \tag{17}$$

The exponent p shows the rate of wake recovery which is supposed as a function of turbulence and can be calculated by Equation (18):

$$p = k_2\left(I_a + I_w\right) \tag{18}$$

where I_a and I_w represent respectively the ambient turbulence and the turbulence generated by the turbine. The turbulence generated by the turbine expressed by Equation (19):

$$I_w = k_3 \frac{C_T}{\max\left(I_a, 0.03\right)}\left(1 - \exp\left(-4\left(\frac{x}{10D}\right)^2\right)\right) \tag{19}$$

The coefficients k_1, k_2, and k_3 are parameters of the Ishihara model, they are given by Equation (20):

$$k_1 = 0.27; k_2 = 6.0; k_3 = 0.004 \tag{20}$$

2.5. Velocity Profile Averaging and Wake Combination

When a WT is subject to the wake of several wind turbines, different methods can be used to combine the different wakes. The most used methods are the energy balance method, the sum of the squares of the speed deficits, the geometric sum, and linear superposition (Katic *et al*. 1987, Renkema, 2007, Shao *et al*. 2019). In this article, the sum of squares model has been used. The Equation of the sum of the squares of the speed deficits is shown in Equation (21):

$$\left(1-\frac{u_i}{u_0}\right)^2 = \sum_{\substack{j=1 \\ j\neq i}}^{N}\left(1-\frac{u_{ij}}{u_0}\right)^2 \tag{21}$$

where u_{ij} is the velocity in the downstream wake region of the turbine j which affects turbine i.

The Larsen and Ishihara wake models describe non-uniform speed profiles. The mean wind speed over the rotor swept area (A) is calculated by using a squared momentum deficit approach (Göçmen *et al*. 2016) as shown in Equation (22):

$$u = \sqrt{\frac{1}{A}\int_A U^2 dA} \tag{22}$$

2.6. Power Calculation

The WT derives its energy from the kinetic energy of the wind, which depends on the mass and speed of the wind. The turbine recovers this kinetic energy by slowing the wind in the space determined by the surface of its rotor. Betz's law determines that a WT can never convert more than 16/27 (or 59%) (Frandsen 1992) [39] of the kinetic energy into mechanical energy. The power calculation can be expressed by Equation (23):

$$P_{wt} = \frac{1}{2}\eta\rho A u^3 \tag{23}$$

with P_{WT} is the power, A is the area of the circle with a radius equal to the length of a blade, u is the wind speed, η is the efficiency of WT and ρ is the density of the air.

When a site is composed of several WTs, the power of the wind farm is calculated by Equation (24):

$$P_{wf} = \sum_{i=1}^{N} P_i \tag{24}$$

where N is the number of turbines and P_i is the power of the i-th turbine.

The efficiency of the WF is expressed in the form of a ratio between the power of the WF and the sum of the powers of the WT taken one by one without a wake effect. This yield is expressed as shown in Equation (25):

$$\eta_{wf} = \frac{P_{wf}}{\sum_{i=1}^{N} P_{si}} \tag{25}$$

with P_{si} is the power of the i-th turbine if it is functioning as a single turbine.

The annual Energy Production (AEP) consists of estimating the annual electricity production of different WTs on the same site for one year. 100% availability is assumed for this estimation. The capacity factor is the ratio between the annual production and the technically possible maximum production of a WT. Capacity factors of 30-40% are considered very high for coastal regions. The hours of operation are the number of hours per year that the wind turbine produces electricity. The number of hours in a year is 8760.

The AEP can be calculated by Equation (26) (Mittal et al. 2016):

$$AEP = T \sum_{i=1}^{directions} \sum_{j=1}^{speed} \sum_{k=1}^{turbines} f_{ijk}\, P_{ijk} \tag{26}$$

where, f_{ijk} is the frequency or probability of wind coming from direction i, with wind speed j on to the wind turbine k, T is the number of hours in one year, and P_{ijk} is the power (in kilowatts) generated by that turbine for the same wind speed and direction.

3. Offshore Wind Farm Site Location and Wind Characteristics

Horns Rev 1 (HR1) is an offshore WF located on a shoal zone in the east of the North Sea about 14 km from the west coast of Denmark as seen in figure 1. It is composed of 80 WTs of 2 MW each manufactured by Vestas. The WT are spread over an area of 5km x 3.9km. The wind farm is arranged in a regular layout in eight lines and ten columns forming a parallelogram with a short side inclined by 7 degrees relative to the north-south direction.

The spacing of the turbines within the WF varies according to the direction. The distance is 7D (560 m) for the two sides of the parallelogram aligned respectively at 270 ° and 353 °. For the first diagonal the distance is 9.4D (750 m) and is aligned at 221 °. For the second diagonal the distance is 10.4 D (833 m) and is aligned at 312 °. The latitude and longitude coordinates of Horns Rev 1 (HR1) are, respectively 55° 30' 11.52" N and 7° 47' 46.931" E. It was the first largest offshore wind farm in the world in 2002 with an installed capacity of 160 MW. The numbers from 1 to 80 are used in the numbering scheme as seen in figure 2 and will be used for referring to some specific turbines in this article.

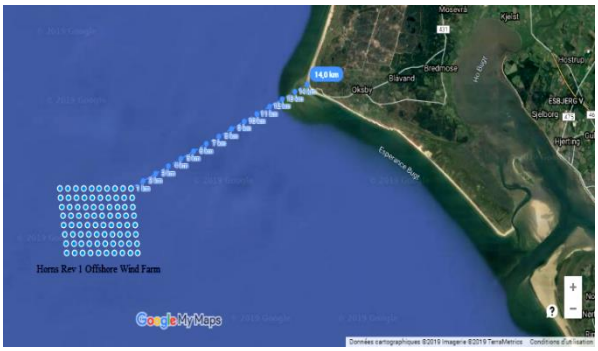

Fig. 1 Map of Horns Rev 1

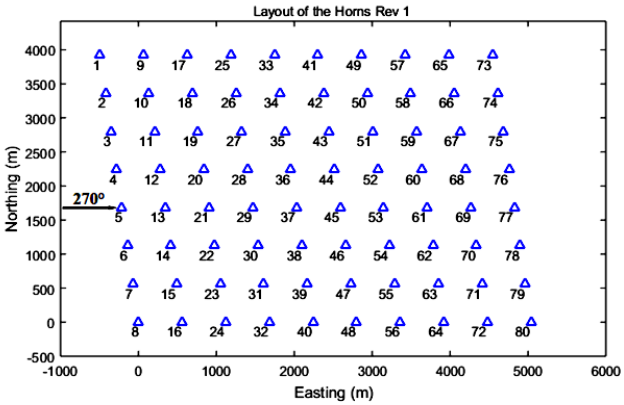

Fig. 2 Numbering scheme of Horns Rev 1

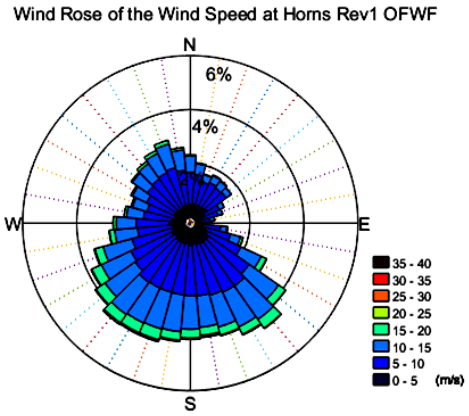

Fig. 4 Wind rose of wind speed distribution in HR 1

Twenty years (1999-2019) of wind speed and direction are taken from the MERRA-2 dataset. The MERRA-2 reanalysis data of long-term datasets are meteorological data taken from meteorological assimilation models, and which have been reworked to ensure long term stability and consistency. MERRA-2 has a sufficiently long history of these data (MERRA-2 2020), and it is available from 1980 to the present. The data are available on regular grids, the spatial resolution of which can be 0.5° × 0.625° (lat x lon), with a spacing of about 55 km for some locations. The spatial interpolation is used to predict the value of the wind speed at the position of Horns Rev1 OWF. This process consists of using points with known values for the estimated values at other unknown points. Spatial interpolation can estimate wind speed and direction at locations without recorded data of MERRA-2 by using known values in nearby to geographic coordinates of a WF (Hassoine *et al.* 2019). The Inverse Distance Weighting (IDW) interpolation method has been used (Ye, 2013); (Van *et al.* 2015) in which sample points are weighted during interpolation in such a way that the influence of one-point relative to other declines with the distance from the unknown point. The hourly wind data (20 years) from the four surrounding MERRA-2 grid (GES DISC 2020) points are used for forecasting hourly wind data of 20 years for Horns Rev1. The wind speed is extrapolated to the hub height of the WTs using the power law.

Figure 3 shows the hourly average wind speed (averaging 175,320 hours) (20 years) at 50 meters, with an average of 9.05 m / s marked by a green line. This wind speed is perfectly suitable for energy production.

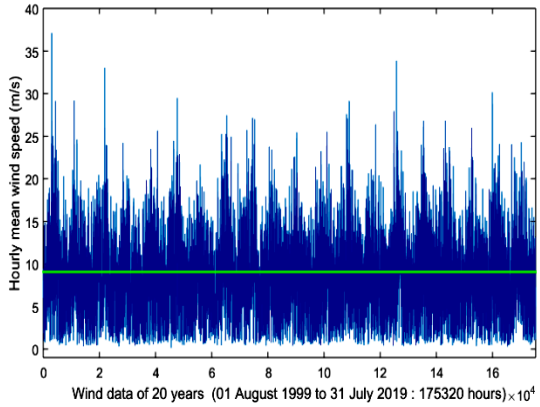

Fig. 3 Wind speed in Horns Rev1, from 01 August 1999 to 31 July 2019

The number of hours during which the wind direction was changed makes it possible to obtain the frequency of wind speeds according to each orientation direction. Therefore, the site has a wind rose as well as an estimated Weibull curve. Regarding the Weibull law, the estimation of the parameters is particularly important to find the values of the shape parameter (k) and the scale parameter (c) in such a way that the Weibull function fits best the available wind data. For our case study, the graphical method has been applied (Deaves & Lines 1997, Kang *et al.* 2018).

The average wind speed at an altitude of 50 meters is 9.05 m/s and becomes 9.36 m/s at the height of the hub (70 m). This average is in perfect agreement with an average of 10 m/s stated by the owner of the Horns Rev 1 offshore wind farm (Vattenfall, owner of 60%) (Vattenfall 2020). Figure 4 shows wind rose of wind speed, from 1999 to 2019. The probabilities for the direction sectors are visualized for grouped data into 36 direction sectors. The prevailing winds come mainly from the southwest during the considered period.

4. Results and Discussion of Investigation of Wake Models in Horns Rev 1

Observational data of Horns Rev 1 is confidential, owners do not share SCADA (Supervisory control and data acquisition) system, except in some very limited cases in the literature, data is limited to specific periods (Jensen *et al.* 2004, Gaumond et al. 2013, Peña et al. 2013, Stevens *et al.* 2016). The available data in the literature has been used to carry out the different simulations.

4.1. Parameters of Models Used for Simulations

The analytical model uses various parameters to include the physical effects. These input parameters are closely related to the turbine model and the kind of wind farm. The main input parameters of the analytical model are the rotor diameter, hub height, distance downstream of the turbine and the axial induction factor. Additional representative parameters are the incoming wind speed, turbulence intensity, and surface roughness. The input parameters data specific to the HR1 have been extracted from (Stevens et al. 2016, Jensen et al. 2004). The Jensen, Larsen, Ishihara, and Frandsen models applied to Horns Rev OWF use the parameters presented in Table 1.

Table 1
Model parameters used for HR1 simulations

Parameters	Value
Wind turbine model	V80 – 2 MW
Rated power (kW)	2000
Cut-in wind speed (m/s)	4
Rated wind speed (m/s)	16
Cut-out wind speed (m/s)	25
Hub height (m)	70
Rotor diameter (m)	80
Thrust coefficient (C_T)	0.78
Turbulence Intensity	7.7%
Roughness length ground (Z_0)	0.002 m
Wake expansion coefficient	0.0382

4.2. Velocity Recovery in the Wake of a Wind Turbine

Simulating the wake of a single turbine provides valuable information to help understand how parameters affect the wake velocity deficit and wake growth behind the turbine. A single wake simulation of a single wind turbine in the HR1 offshore wind farm has been performed for each wake model. The simulation is also compared with the single wake simulation of the onshore wind farm which was performed by Tong et al. (Tong *et al.* 2012) in flat terrain where one single GE 2.5 MW - 100 m turbine is installed. The thrust coefficient and the ambient turbulence are assumed to be constant at 0.13 and 0.82 (onshore), respectively.

Figures 5 and Fig 6 plot the wake growth and wake velocity predicted by the four different analytical wake models for the V80 - 2 MW turbine (HR1) and the GE 2.5MW-100 turbine (Tong). It is seen that, over the whole flow field, the Frandsen model forecasts the largest wake velocity and the Larsen model predicts the largest wake diameter. The Ishihara model forecasts the lowest wake speed. Yet, it gives the highest wake recovery rate. According to Tong *et al.* (Tong *et al.* 2012). This is due to the greater mixing of the wake with the upper layers of the atmospheric boundary layer (ABL), which is facilitated by the turbulence induced by the turbine.

It is clear from figure 5 that the wake expansion behind the WT in the Tong simulations is larger than the wake expansion behind the WT in HR1. This can be explained by the fact that the onshore wind farm has a high intensity of turbulence and a high thrust coefficient, which are 0.13 and 0.82, respectively. In contrast, Horns Revs 1 has a low intensity of turbulence and a moderate thrust coefficient, which are 0.077 and 0.78, respectively.

The wake of HR1 undergoes a progressive expansion that accompanies the reduction of the velocity deficit. Recovery of the velocity reaches 80% from 10 rotor diameters. This distance depends on the turbulent intensity of the flow. An interesting phenomenon that can be seen in figure 6 is that the Jensen model outperforms the Larsen model beyond 15D (1200 m). Frandsen's model predicts the lowest velocity deficit ranging from 0.74 to 0.96. The Jensen and Ishihara models predict at a distance of 7D (560 m) the same velocity deficit with a value of 0.74.

4.3. Power Deficit as a Function of Wind Direction

The wind is an inherently very complex aerodynamic phenomenon. Wind speed and direction have a fluctuating Spatio-temporal character. Therefore, the power delivered by the offshore wind farm is sensitive to the direction of the wind. The simulations for a westerly wind (270°) of the fourth row of HR1 were studied and compared with the measurements (Barthelmie *et al.* 2009a) and with the results of previous studies (Barthelmie *et al.* 2000a, Stevens *et al.* 2016).

Prior to comparing the model simulations with the wind farm data. The sensitivity of the power deficit to wind direction in the range 210°- 330° was simulated and plotted in a single figure. The simulation is performed by the Jensen model under a constant velocity of 8.5 m/s. Figure 7 shows a comparison of normalized power to the power of turbine WT4.

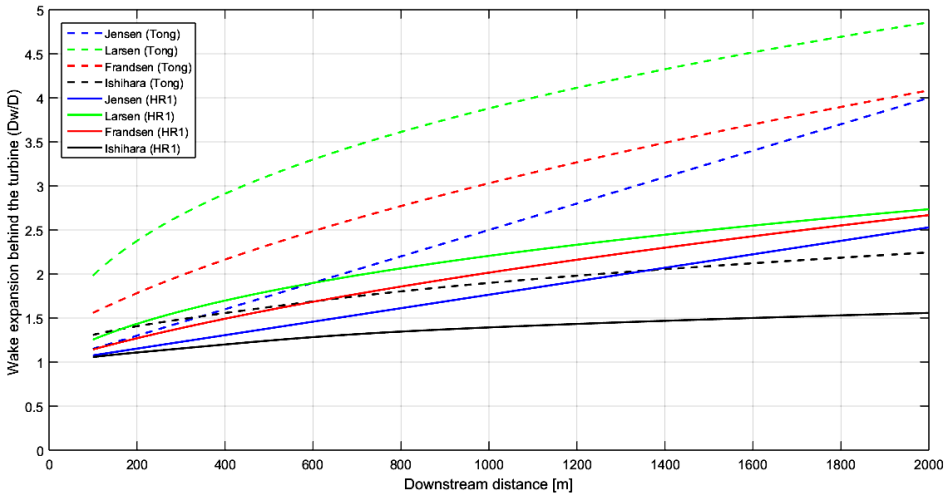

Fig. 5 Wake expansion in HR1 behind the turbine (normalized to rotor diameter D)

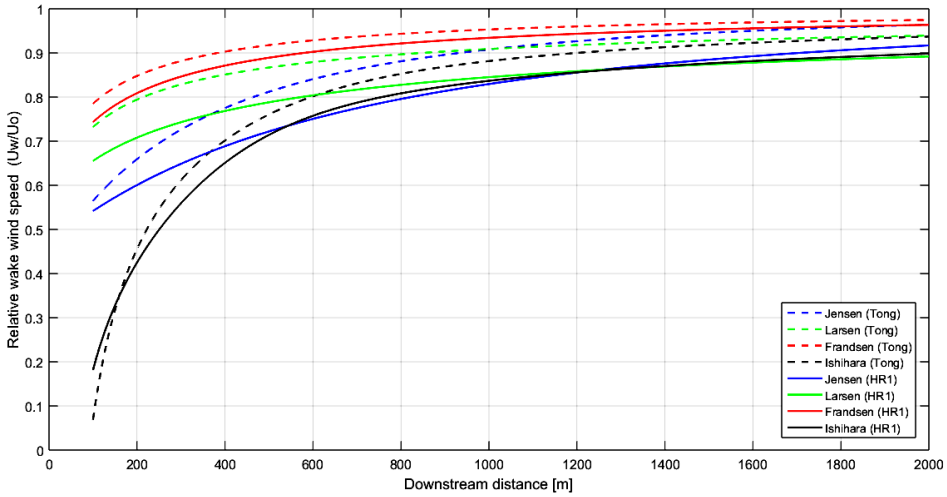

Fig. 6 Wake speed in HR1 (normalized to free stream wind speed U0)

Figure 7 reveals that in the 270° direction, the wakes of the 10 turbines are directly superimposed, the first highest limit of power deficits is reached. The 225° and 315° directions show that the second highest limit of power deficits is reached 50%. According to Pena et al. (Pena *et al.* 2014). This is due to the second turbine in the row is almost directly downstream of the first turbines in the upper and lower rows. When the wind arrives in the directions of 255° and 285°, the first three turbines in the row are not affected by the wake of the other turbines, resulting in the lowest deficit of 30%.

To assess the ability of models to predict wake losses, seven cases are analyzed in the range 255° to 285°, for a wind speed of 8.0 ± 0.5 m/s. The data used for this study cover the period from January 1, 2005, to December 31, 2005, with the deviation of observations is ±2.5 ° (Berthalmie *et al*. 2009 a). Figure 8 shows various wind directions from 255 ° to 285 ° in the 4th row.

Note, Stevens has performed the simulations by using the coupled wake boundary layer (CWBL) model and Jensen model. Berthalmie has performed the simulations by using the NTUA, ECN, and GH WindFarmer model. The CWBL model has been developed by coupling wake model and boundary layer (Stevens et al. 2015). According to Berthalmie *et al.* (Berthalmie *et al.* 2009 b). NTUA CFD model based on solving the 3D Reynolds averaged incompressible Navier-Stokes Equations. ECN's wake model is based on parabolized Navier-Stokes Equations. GH WindFarmer is based on the eddy viscosity wake model is a CFD calculation representing the development of the velocity deficit using a finite-difference solution of the Navier-Stokes Equations in axis-symmetric co-ordinates. Comparisons of the simulation results with measurements are given in Figures 9 to 15.

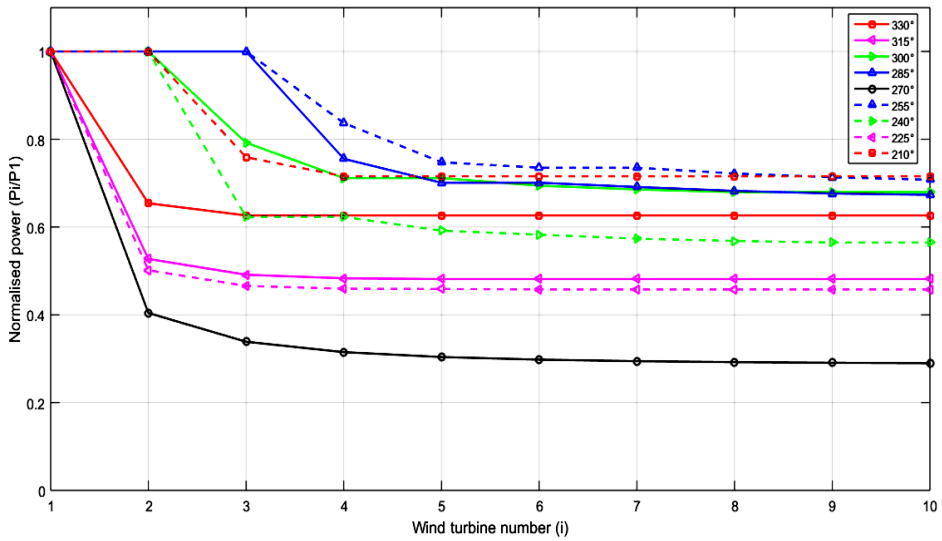

Fig. 7 Normalized power in the fourth row, from 210 ° to 330 ° (normalized to the power of WT4)

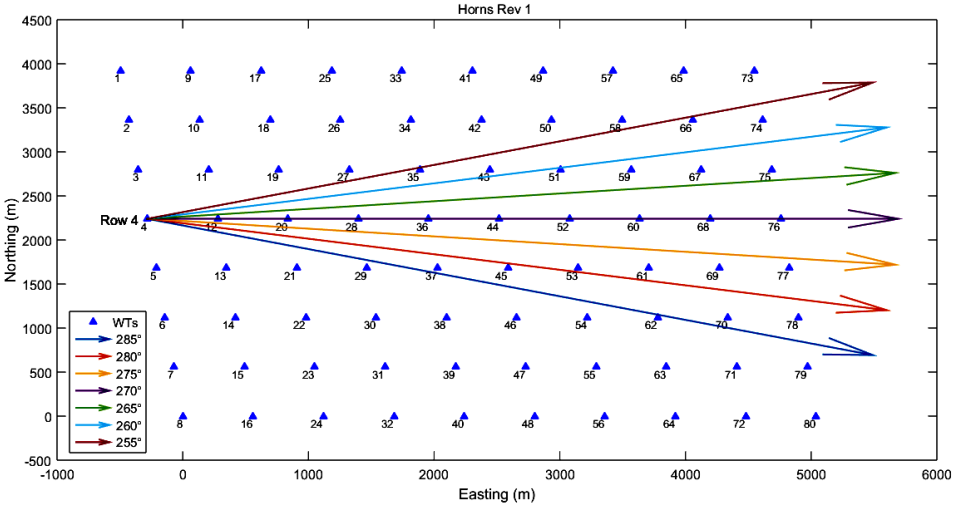

Fig. 8 Wind direction from 255 ° to 285 ° in the 4th row

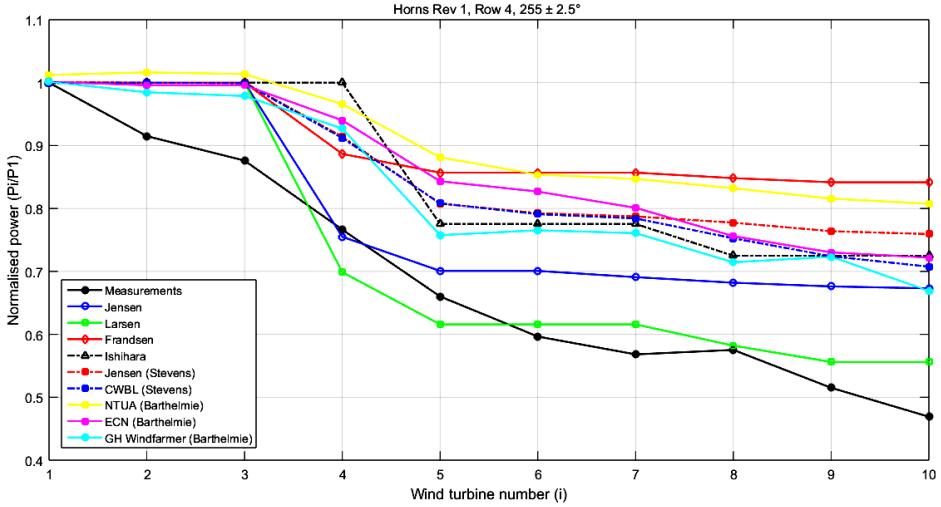

Fig. 9 Normalized power in the fourth row for the direction 255 °

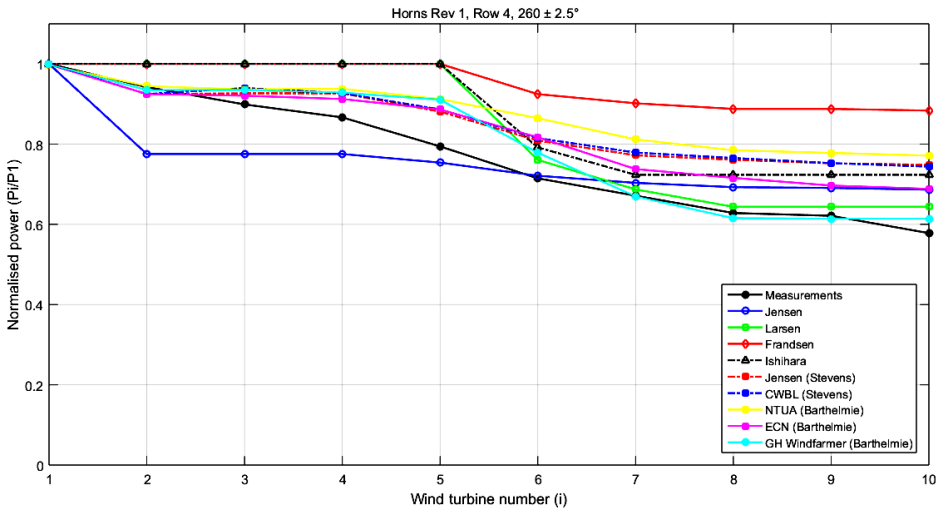

Fig. 10 Normalized power in the fourth row for the direction 260 °

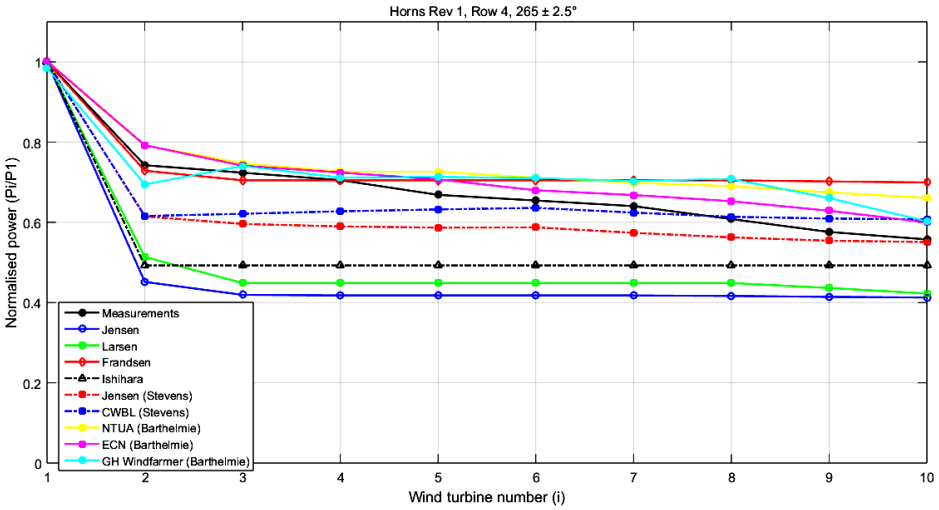

Fig. 11 Normalized power in the fourth row for the direction 265°

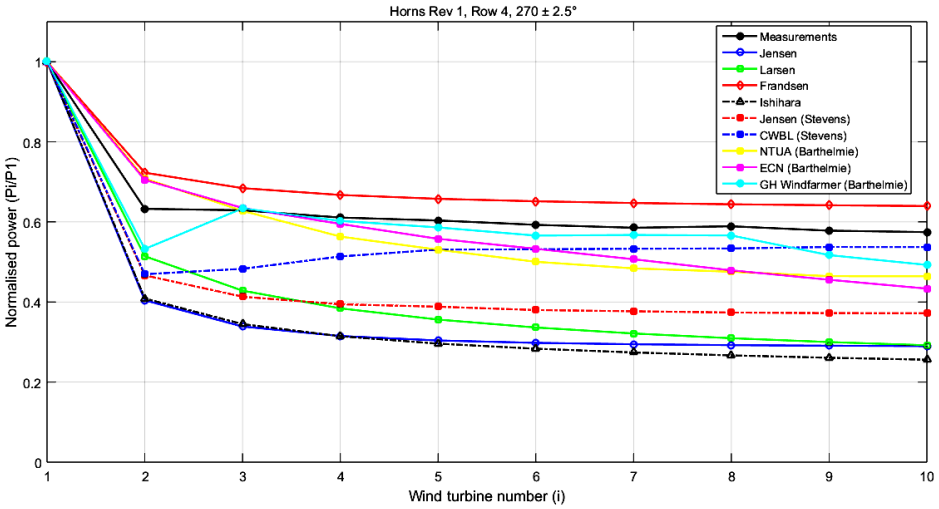

Fig. 12 Normalized power in the 4th row for the direction 270 °

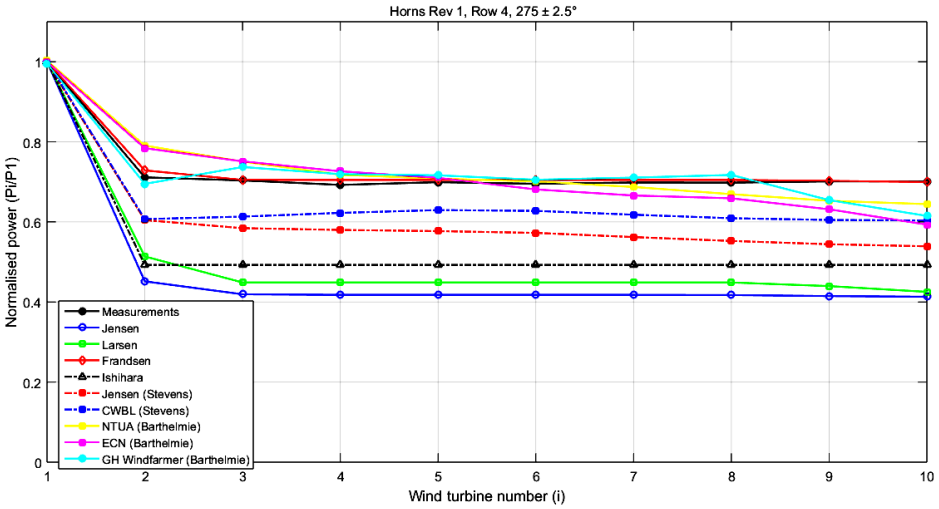

Fig. 13 Normalized power in the fourth row for the direction 275 °

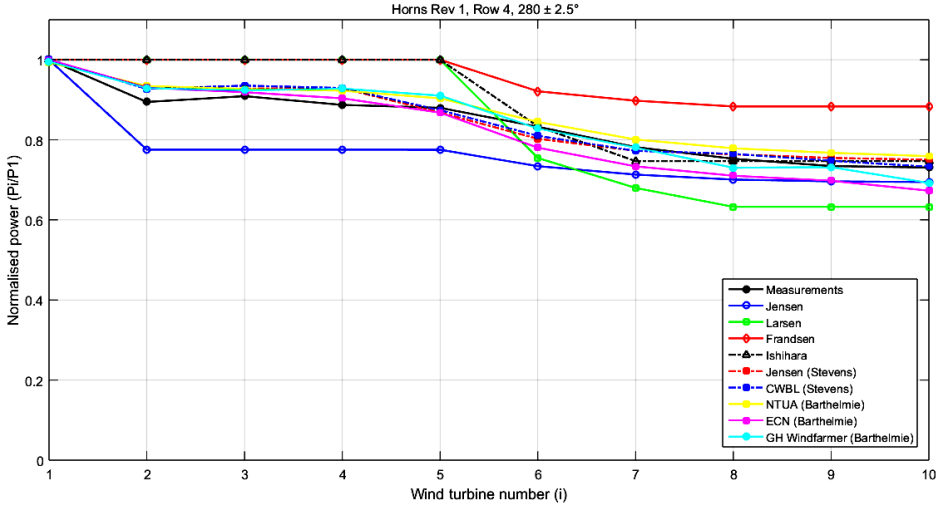

Fig. 14 Normalized power in the fourth row for the direction 280°

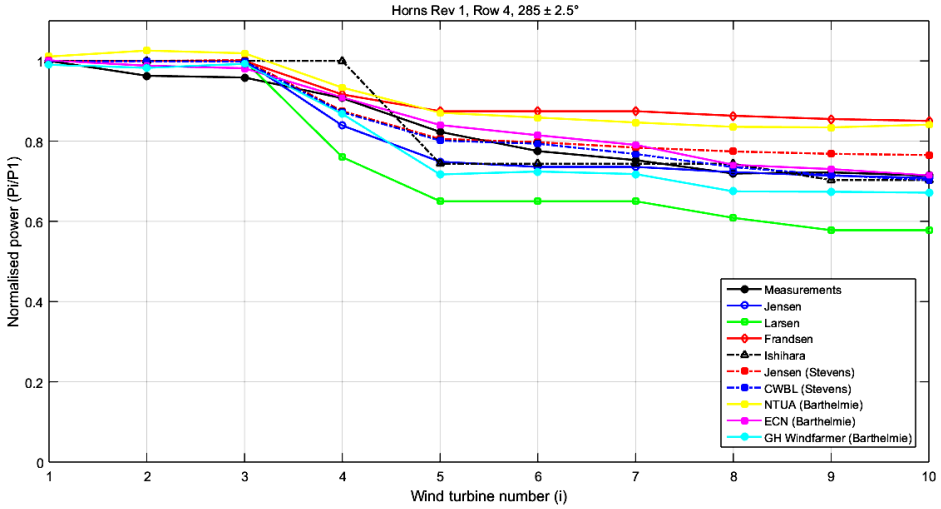

Fig. 15 Normalized power at the fourth row for the direction 285 °

To perform a quantitative analysis, the root mean square error (RMSE), and the mean absolute percentage error (MAPE) are used to measure the difference between predictions and observations to determine the performance of the model. Their definitions are as below:

$$RMSE = \sqrt{\frac{1}{n}\sum_{i}^{n}\left(NP_{m,i} - NP_{e,i}\right)^{2}} \quad (27)$$

$$MAPE = \frac{1}{n}\sum_{i}^{n}\left|\frac{NP_{m,i} - NP_{e,i}}{NP_{m,i}}\right| \times 100\% \quad (28)$$

where NPm,i is the normalized measured power of the ith turbine, NPe,i is the corresponding normalized estimated power, n is the number of data points used in the validation. The RMSE and MAPE of different model simulation results are listed in Tables 2 and 3, respectively. The lowest RMSE and MAPE errors indicate a good agreement between measurements and predictions.

The results of the quantitative analysis indicate that the quality of the estimate of each model strongly depends on the wind direction. The results also show that the models are not able to produce the best forecasts for all wind directions. In fact, each model is more or less good for a certain direction. However, it can be seen that the great drop in power occurs in a narrow sector of 265° to 275° which is captured by all models. In particular, for 265° and 285° ECN model gives a good estimation and the Frandsen model simulates correctly the normalized power of 275°. Moreover, GH model is more favorable for wind directions of 260° and 270°. It is also important to note that the 255° direction is captured well by the Larsen model and CWBL model performs well for 280°.

Table 2
Comparison of RMSE for different models

Model	RMSE						
	255 °	260 °	265 °	270 °	275 °	280 °	285 °
Jensen	0.113	0.086	0.226	0.271	0.265	0.086	0.039
Larsen	**0.064**	0.090	0.196	0.231	0.235	0.098	0.115
Frandsen	0.233	0.200	0.073	0.059	**0.008**	0.114	0.093
Ishihara	0.172	0.110	0.162	0.285	0.196	0.069	0.045
Jensen (Stevens)	0.184	0.097	0.080	0.196	0.126	0.022	0.037
CWBL (Stevens)	0.168	0.099	0.061	0.086	0.081	**0.021**	0.023
NTUA (Barthelmie)	0.230	0.122	0.063	0.083	0.039	0.026	0.082
ECN (Barthelmie)	0.183	0.071	**0.035**	0.080	0.053	0.036	**0.022**
GH (Barthelmie)	0.148	**0.049**	0.055	**0.047**	0.035	0.024	0.049

Table 3
Comparison of MAPE for different models

Model	MAPE %						
	255 °	260 °	265 °	270 °	275 °	280 °	285 °
Jensen	9.59	7.02	20.91	25.69	25.13	7.63	2.94
Larsen	**5.22**	6.62	18.11	21.54	22.29	9.29	10.16
Frandsen	20.47	17.69	5.48	5.60	**0.61**	10.65	7.73
Ishihara	15.59	9.69	14.42	26.91	18.66	4.99	3.46
Jensen (Stevens)	16.61	8.22	6.60	18.60	11.85	1.95	3.36
CWBL (Stevens)	15.38	8.53	4.67	7.26	7.65	**1.67**	2.01
NTUA (Barthelmie)	21.04	10.27	5.50	7.29	3.14	2.42	7.41
ECN (Barthelmie)	16.71	6.20	**3.19**	6.51	4.28	3.11	**1.75**
GH (Barthelmie)	13.40	**3.44**	4.79	**3.42**	2.71	1.93	4.29

However, when each model is taken alone. The agreement between simulations and Horns Rev data is less favorable for the wind directions between 255° and 285°. According to Stevens *et al.* (Stevens *et al.* 2016). The differences between the field data and the model outputs are not only caused by the limitations of the model but can also be assigned to the limitations of the capacity to specify the model inputs. In particular, figures 9 to 15 clearly show that, within the same model, the choice of wind direction influences the model calibration.

Moreover, a comparison based MAPE was made between Jensen, Larsen, Ishihara, and Frandsen model. Table 4 reports the ranking results. The rank shows that the Frandsen model performs well for the wind directions between 265 ° and 275 °.

4.4. Efficiency as a Function of Wind Direction

To understand how the variability of the wind direction affects the total output of all the turbines in the Horns Rev 1, the evolution of the efficiency has been simulated relative to the directions of the interval 0° to 360°. The models are compared with SCADA measurements (Hasager 2015) for a wind speed of 8.0 ± 0.5 m/s. The wind directions are divided into 72 parts. The results were also compared with Hasager's and Peña's simulations (Hasager 2015, Peña 2104). Peña's simulations have been performed by the Jensen model and Hasager's simulations have been carried out by using a CFD tool named GCL. Figure 16 shows the simulation of the efficiency in the interval 0 to 360 °

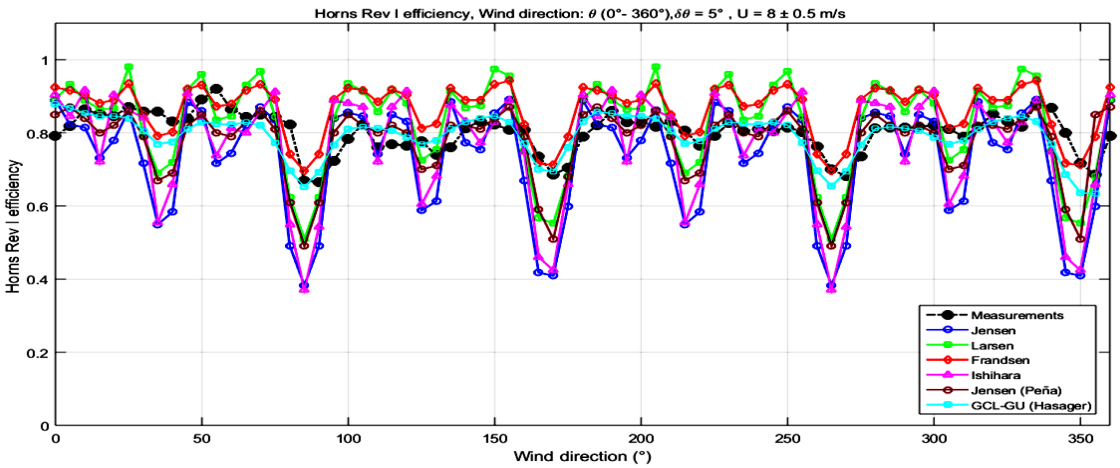

Fig. 16 Horns Rev1 efficiency for inflow sector 0° to 360°; comparison of models and data for U = 8.0 ± 0.5 m/s

Table 4
Comparison of four analytical wake models

Model	Rank						
	255 °	260 °	265 °	270 °	275 °	280 °	285 °
Jensen	2	2	4	3	4	2	1
Larsen	1	1	3	2	3	3	4
Frandsen	4	4	**1**	**1**	**1**	4	3
Ishihara	3	3	2	4	2	1	2

SCADA measurements show four sectors that give high deficits. These sectors correspond to the four main directions of the park and they correspond, respectively, to 90°, 173°, 270°, and 353°. All four models predict these sectors. The diagonal sectors corresponding, respectively, to 41°, 132°, 221°, and 312 ° are also captured by the models. These sectors are marked by relatively high deficits. The main and diagonal directions are shown in Figure 17. The efficiency of 0° to 360° and of main and diagonal directions for all models is displayed in Table 5.

It is also interesting to note that main and diagonal directions correspond to full-wake conditions. The results show that a number of the models significantly over predict the maximum power losses when compared to the SCADA measurements. In contrast, the GCL model simulates the power losses exactly.

An interesting result, which can be seen in Table 5, is that the maximum loss has been estimated for the principal and diagonal directions, but when the losses are estimated for 0° to 360° a compensation effect between directions is observed. For example, Jensen's model predicts a 46% loss for diagonal sectors and a 62% loss for the main sector. However, for 0° to 360°, this model predicted a 27 % loss.

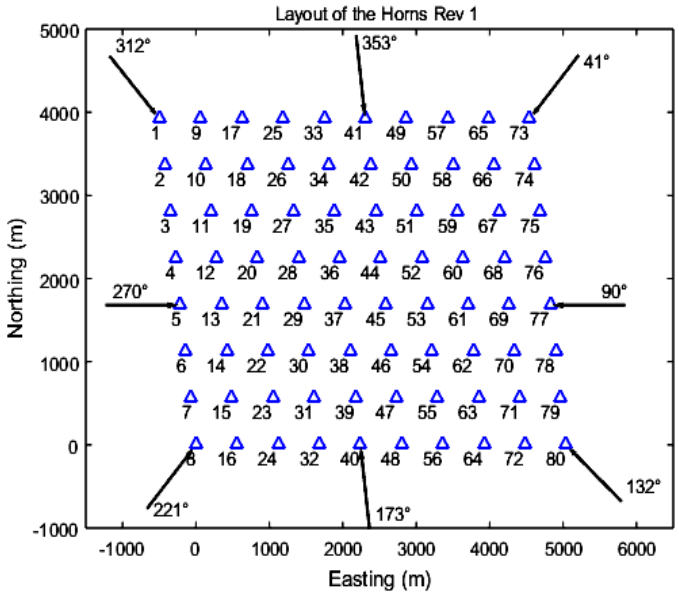

Fig. 17 Main and diagonal directions of Horns Rev1

Table 5
The Efficiency in the Main and Diagonal Directions of Horns Rev 1

Direction	Spacing	Measurements	Jensen	Larsen	Frandsen	Ishihara	Jensen (Peña)	GCL-GU (Hasager)
0 ° - 360 °	-	0.80	0.73	0.82	0.86	0.76	0.77	0.79
41 °	9.4 D	0.85	0.54	0.69	0.79	0.55	0.67	0.76
90 °	7 D	0.66	0.38	0.50	0.69	0.37	0.49	0.65
132 °	10.4 D	0.77	0.58	0.72	0.81	0.60	0.70	0.76
173 °	7 D	0.68	0.40	0.55	0.71	0.42	0.51	0.69
221 °	9.4 D	0.80	0.54	0.69	0.79	0.55	0.67	0.77
270 °	7 D	0.70	0.38	0.50	0.69	0.37	0.49	0.65
312 °	10.4 D	0.81	0.58	0.72	0.81	0.60	0.70	0.76
353 °	7 D	0.71	0.40	0.55	0.71	0.42	0.51	0.63

Table 6
Power output *and AEP* of Horns Rev 1

	Power output [MW]	AEP [GWh]	Relative Difference of AEP [%]
Horns Rev 1	66.21	580	-
Feng (2015)	78.79	690.2	+ 19
Hou (2017)	84.22	737.78	+ 27.2
Wade (2019)	72.68	636.7	+ 9.77
Sørensen (2021)	68.26	598	+ 3.1
Jensen	77.26	676.79	+ 16.68
Larsen	74.48	652.44	+ 12.49
Frandsen	81.48	713.76	+ 23.06
Ishihara	76.90	673.64	+ 16.14

4.5. Power Output of Horns Rev 1 Offshore Wind Farm

In this section, the output power and annual energy production (AEP) of the Horns Rev 1 offshore wind farm have been calculated and compared with the measurements (Sørensen & Larsen, 2021) and also with the results of previous studies (Feng & Shen 2015, Hou et al. 2017, Wade et al. 2019, Sørensen & Larsen, 2021). The AEP was investigated by using four wake models under twenty years of wind data. Weibull distribution has been used to express the wind speed frequency distribution. Moreover, the shape parameter (k= 2.4258) and the scale parameter (c = 10.5652 m/s) have been calculated at 70 m from sea level with an average wind speed of 9.3678 m/s.

The power of each turbine and the output power of HR1 are calculated using Equations (23) and (24), respectively. The annual energy production is estimated by using Equation (26). The power output and AEP of Horns Rev 1 are shown in Table 6.

The comparison between the calculated and reported power output of Horns Revs 1 showed that models significantly over predict the power output in comparison with the measurements. Moreover, the four model differences ranged from - 8.27 MW (12.49%) to 15.27 MW (23.06%) for the Larsen and Frandsen models, respectively. Therefore, to have an agreement between the predictions and the field data, the input parameters of the models must be estimated and calibrated.

5. Conclusions

This paper presents an approach to investigate the wake effect inside OWFs. A comparative study of wake models within an OWF, has been conducted using the models of Jensen, Larsen, Ishihara, and Frandsen. These wake models have been evaluated in many situations and configurations, to highlight wake effects on the power output of turbines inside the WF. The single and multiple wakes are also studied.

The total power of Horns Rev 1 OWF has been evaluated with hourly wind data based on 20 years (1999-2019) of MERRA-2 data. The ability of models has also been discussed. In this paper, the obtained results have provided a better understanding of the phenomena related to the variability and interactions of wind wakes within an OWF, which could thus be better taken into account when designing WFs. The simulated results are promising and show that the proposed work is useful. All models offer a good description of the wake effect, each model is also suitable to the real conditions of existing offshore wind farms. However, the input parameters of models need to be estimated and calibrated. In the ongoing research, realistic wind conditions will be taken into consideration in the OWF by using more complex wake models such as CFD based models.

Conflicts of Interest

The authors declare that they have no conflicts of interest.

References

Barthelmie, R., Frandsen, S. T., Hansen, K., Schepers, J., Rados, K., Schlez, W., & Neckelmann, S. (2009 a). Modelling the impact of wakes on power output at Nysted and Horns Rev. In European Wind Energy Conference (pp. 1-10).

Barthelmie, R, Hansen, K., Frandsen, S., Rathmann, O., Schepers, J., & Schlez, W. et al. (2009 b). Modelling and measuring flow and wind turbine wakes in large wind farms offshore. Wind Energy, 12(5), 431-444. https://doi.org/10.1002/we.348.

Bastankhah, M., & Porté-Agel, F. (2014). A new analytical model for wind-turbine wakes. Renewable Energy, 70, 116-123. https://doi.org/10.1016/j.renene.2014.01.002.

Brun, C., Tenchine, D., & Hopfinger, E. (2004). Role of the shear layer instability in the near wake behavior of two side-by-side circular cylinders. Experiments In Fluids, 36(2), 334-343. https://doi.org/10.1007/s00348-003-0726-6.

Chowdhury, S., Zhang, J., Messac, A., & Castillo, L. (2012). Unrestricted wind farm layout optimization (UWFLO): Investigating key factors influencing the maximum power generation. Renewable Energy, 38(1), 16-30. https://doi.org/10.1016/j.renene.2011.06.033.

Crasto, G., Gravdahl, A., Castellani, F., & Piccioni, E. (2012). Wake Modeling with the Actuator Disc Concept. Energy Procedia, 24, 385-392. https://doi.org/10.1016/j.egypro.2012.06.122.

Deaves, D., & Lines, I. (1997). On the fitting of low mean windspeed data to the Weibull distribution. Journal Of Wind Engineering And Industrial Aerodynamics, 66(3), 169-178. https://doi.org/10.1016/s0167-6105(97)00013-5.

Feng, J., & Shen, W. (2015). Modelling Wind for Wind Farm Layout Optimization Using Joint Distribution of Wind Speed and Wind Direction. Energies, 8(4), 3075-3092. https://doi.org/10.3390/en8043075.

Frandsen, S., Barthelmie, R., Pryor, S., Rathmann, O., Larsen, S., Højstrup, J., & Thøgersen, M. (2006). Analytical modelling of wind speed deficit in large offshore wind farms. Wind Energy, 9(1-2), 39-53. https://doi.org/10.1002/we.189.

Frandsen, S. (1992). On the wind speed reduction in the center of large clusters of wind turbines. Journal Of Wind Engineering And Industrial Aerodynamics, 39(1-3), 251-265. https://doi.org/10.1016/0167-6105(92)90551-k.

Gao, X., Yang, H., & Lu, L. (2016). Optimization of wind turbine layout position in a wind farm using a newly-developed two-dimensional wake model. Applied Energy, 174, 192-200. https://doi.org/10.1016/j.apenergy.2016.04.098.

García, L., Vatn, M., Mühle, F., & Sætran, L. (2017). Experiments in the wind turbine far wake for the evaluation of an analytical wake model. Journal Of Physics: Conference Series, 854, 012015. https://doi.org/10.1088/1742-6596/854/1/012015.

Gaumond, M., Réthoré, P., Ott, S., Peña, A., Bechmann, A., & Hansen, K. (2013). Evaluation of the wind direction uncertainty and its impact on wake modeling at the Horns

Rev offshore wind farm. Wind Energy, 17(8), 1169-1178. https://doi.org/10.1002/we.1625.

GES DISC. Disc.sci.gsfc.nasa.gov. (2020). Retrieved 15 December 2020, from https://disc.sci.gsfc.nasa.gov/datasets?keywords=%22MERRA-2%22&page=1&source=Models%2FAnalyses%20MERRA-2.

Göçmen, T., Laan, P., Réthoré, P., Diaz, A., Larsen, G., & Ott, S. (2016). Wind turbine wake models developed at the technical university of Denmark: A review. Renewable And Sustainable Energy Reviews, 60, 752-769. https://doi.org/10.1016/j.rser.2016.01.113.

Hamilton, N., Bay, C., Fleming, P., King, J., & Martínez-Tossas, L. (2020). Comparison of modular analytical wake models to the Lillgrund wind plant. Journal Of Renewable And Sustainable Energy, 12(5), 053311. https://doi.org/10.1063/5.0018695.

Hasager, C. B., Giebel, G. (2015). EERA DTOC final summary report. EERA DTOC - European Energy Research Alliance - Design Tool for Offshore Wind Farm Cluster..

Hassoine, M., Lahlou, F., Addaim, A., & Madi, A. (2019). A Novel Evaluation of Wind Energy Potential in Essaouira Offshore Wind Farm, using Genetic Algorithm and MERRA-2 Reanalysis Data. 2019 5Th International Conference On Optimization And Applications (ICOA). https://doi.org/10.1109/icoa.2019.8727669.

Hou, P., Hu, W., Soltani, M., Chen, C., & Chen, Z. (2017). Combined optimization for offshore wind turbine micro siting. Applied Energy, 189, 271-282. https://doi.org/10.1016/j.apenergy.2016.11.083.

Ishihara, T., Yamaguchi, A., and Fujino, Y., 2004. Development of a New Wake Model Based on a Wind Tunnel Experiment. Global Wind Power.

Jensen, L., Mørch, C., Sørensen, P., Svendsen, K. H. 2004. Wake measurements from the Horns Rev wind farm. EWEC 2004, 22-25 November 2004. London, United Kingdom.

Jensen, N. O. 1983. A note on wind generator interaction. Risø National Laboratory. Risø-M, No. 2411.

Kang, D., Ko, K., & Huh, J. (2018). Comparative Study of Different Methods for Estimating Weibull Parameters: A Case Study on Jeju Island, South Korea. Energies, 11(2), 356. https://doi.org/10.3390/en11020356.

Katic, I., Højstrup, J., & Jensen, N. O. (1987). A Simple Model for Cluster Efficiency. In W. Palz, & E. Sesto (Eds.), EWEC'86. Proceedings. Vol. 1 (pp. 407-410). A. Raguzzi.

Larsen, G. C. 1988. A Simple Wake Calculation Procedure. Risø National Laboratory. Risø-M, No. 2760.

Larsen, G. C. 2009. A simple stationary semi-analytical wake model. Risø National Laboratory for Sustainable Energy, Technical University of Denmark. Denmark. Forskningscenter Risoe. Risoe-R, No. 1713(EN).

Machefaux, E. 2015. Multiple Turbine Wakes. DTU Wind Energy. DTU Wind Energy PhD, No. 0043(EN).

MERRA-2. Gmao.gsfc.nasa.gov. (2020). Retrieved 15 December 2020, from https://gmao.gsfc.nasa.gov/reanalysis/MERRA-2/.

Mittal, P., Kulkarni, K., & Mitra, K. (2016). A novel hybrid optimization methodology to optimize the total number and placement of wind turbines. Renewable Energy, 86, 133-147. https://doi.org/10.1016/j.renene.2015.07.100.

Peña, A., Réthoré, P-E., Hasager, C. B., & Hansen, K. S. (2013). Results of wake simulations at the Horns Rev I and Lillgrund wind farms using the modified Park model. DTU Wind Energy. DTU Wind Energy E, No. 0026(EN).

Power plants: Horns Rev 1 - Vattenfall. Powerplants.vattenfall.com. (2020). Retrieved 30 May 2020, from https://powerplants.vattenfall.com/horns-rev.

Renkema, D.J. 2007. Validation of wind turbine wake models: Using wind farm data and wind tunnel measurements. Master of Science Thesis. Delft University of Technology.

Richmond, M., Antoniadis, A., Wang, L., Kolios, A., Al-Sanad, S., & Parol, J. (2019). Evaluation of an offshore wind farm computational fluid dynamics model against operational site data. Ocean Engineering, 193, 106579. https://doi.org/10.1016/j.oceaneng.2019.106579.

Shao, Z., Wu, Y., Li, L., Han, S., & Liu, Y. (2019). Multiple Wind Turbine Wakes Modeling Considering the Faster Wake Recovery in Overlapped Wakes. Energies, 12(4), 680. https://doi.org/10.3390/en12040680.

Sørensen, J., & Larsen, G. (2021). A Minimalistic Prediction Model to Determine Energy Production and Costs of Offshore Wind Farms. Energies, 14(2), 448. https://doi.org/10.3390/en14020448.

Stevens, Richard J. A. M., Dennice F. Gayme, and Charles Meneveau. 2016. "Generalized Coupled Wake Boundary Layer Model: Applications And Comparisons With Field And LES Data For Two Wind Farms". Wind Energy 19 (11): 2023-2040. doi:10.1002/we.1966.

Sun, H., & Yang, H. (2018). Study on three wake models' effect on wind energy estimation in Hong Kong. Energy Procedia, 145, 271-276. https://doi.org/10.1016/j.egypro.2018.04.050.

Tian, L., Zhu, W., Shen, W., Zhao, N., & Shen, Z. (2015). Development and validation of a new two-dimensional wake model for wind turbine wakes. Journal Of Wind Engineering And Industrial Aerodynamics, 137, 90-99. https://doi.org/10.1016/j.jweia.2014.12.001.

Tong, W., Chowdhury, S., Zhang, J., & Messac, A. (2012, September). Impact of different wake models on the estimation of wind farm power generation. In 12th AIAA Aviation Technology, Integration, and Operations (ATIO) Conference and 14th AIAA/ISSMO. Multidisciplinary Analysis and Optimization Conference (p. 5430).

Van Ackere, S., Van Eetvelde, G., Schillebeeckx, D., Papa, E., Van Wyngene, K., & Vandevelde, L. (2015). Wind Resource Mapping Using Landscape Roughness and Spatial Interpolation Methods. Energies, 8(8), 8682-8703. https://doi.org/10.3390/en8088682.

Vermeer, L., Sørensen, J., & Crespo, A. (2003). Wind turbine wake aerodynamics. Progress In Aerospace Sciences, 39(6-7), 467-510. https://doi.org/10.1016/s0376-0421(03)00078-2.

Vestas V80 Offshore - 2,00 MW - Éolienne. Fr.wind-turbine-models.com. Retrieved 13 September 2020, from https://fr.wind-turbine-models.com/turbines/668-vestas-v80-offshore.

Wade, B., Pereira, R., & Wade, C. (2019). Investigation of offshore wind farm layouts regarding wake effects and cable topology. Journal Of Physics: Conference Series, 1222, 012007. https://doi.org/10.1088/1742-6596/1222/1/012007

Ye, W.. (2013) Spatial Variation and Interpolation of Wind Speed Statistics and Its Implication in Design Wind Load. Electronic Thesis and Dissertation Repository.1254. https://ir.lib.uwo.ca/etd/1254.